Search for Ultralight Dark Matter with a Frequency Adjustable Diamagnetic Levitated Sensor

Rui Li(李睿)[1,2], Shaochun Lin(林劭春)[1,2], Liang Zhang(张亮)[1,2], Changkui Duan(段昌奎)[1,2], Pu Huang(黄璞)[3*], and Jiangfeng Du(杜江峰)[1,2]

[1]*CAS Key Laboratory of Microscale Magnetic Resonance and School of Physical Sciences, University of Science and Technology of China, Hefei 230026, China*
[2]*CAS Center for Excellence in Quantum Information and Quantum Physics, University of Science and Technology of China, Hefei 230026, China*
[3]*National Laboratory of Solid State Microstructures and Department of Physics, Nanjing University, Nanjing 210093, China*

(Received 24 March 2023; accepted manuscript online 16 May 2023)

Among several dark matter candidates, bosonic ultra-light (sub-meV) dark matter is well motivated because it could couple to the Standard Model and induce new forces. Previous MICROSCOPE and Eöt–Wash torsion experiments have achieved high accuracy in the sub-1 Hz region. However, at higher frequencies there is still a lack of relevant experimental research. We propose an experimental scheme based on the diamagnetic levitated micromechanical oscillator, one of the most sensitive sensors for acceleration sensitivity below the kilohertz scale. In order to improve the measurement range, we utilize a sensor whose resonance frequency ω_0 could be adjusted from 0.1 Hz to 100 Hz. The limits of the coupling constant g_{B-L} are improved by more than 10 times compared to previous reports, and it may be possible to achieve higher accuracy by using the array of sensors in the future.

DOI: 10.1088/0256-307X/40/6/069502

So far, there have been many astronomical[1,2] and cosmological observations[3] that prove the existence of cold dark matter.[4] However, the specific parameters of dark matter, especially the quality, are still highly uncertain.[5] Many direct detection studies have assumed that dark matter is composed of supersymmetric fermions, but up to date there has not been enough evidence appearing. Now the focus of research is gradually shifting to ultralight bosons and the quality range is approximately $10^{-22}\,\text{eV} < m_\phi < 0.1\,\text{eV}$.[6,7] For ultralight bosons with a mass less than 1 eV, due to their high particle number density, they behave like a classical field. Due to the viral theorem, if the dark matter (DM) has virialized to the Galaxy, it will be moving with a typical speed $v_{\rm DM} \approx 10^5\,\text{m/s}$.[8–10] This corresponds to Compton frequency $\omega_{\rm s} = m_\phi/\hbar$ and de Broglie wavelength $\lambda_{\rm DM} = hc^2/(m_\phi v_{\rm DM})$.

According to the previous reports, ADMX[11] can search for the Peccei–Quinn axion in the mass range $10^{-6}\,\text{eV} < m_\phi < 10^{-3}\,\text{eV}$.[12,13] Researchers have recently reported the pseudoscalar axion-like ultralow-mass bosons (ULMBs) with masses between $10^{-23}\,\text{eV}$ and $10^{-18}\,\text{eV}$[14–16] and scalar dilaton ULMBs with masses between $10^{-21}\,\text{eV}$ and $10^{-5}\,\text{eV}$ by using ultrastable clocks[17,18] and gravitation wave detectors.[19]

When DM is a vector field coupling to a conserved current, corresponding to the baryon number minus lepton number ($B-L$ charge) in the Standard Model (SM). The Lagrangian in this case can be written as[20]

$$\mathcal{L} = -\frac{1}{4}F_{\mu\nu}F^{\mu\nu} - \frac{1}{2}m_\phi^2 A^2 + ig_{B-L}A_\mu \overline{n}\gamma^\mu n, \qquad (1)$$

where n is the neutron field and the DM field couples directly to the number of neutrons, g_{B-L} is the coupling strength. Using the Lorentz gauge and the plane wave approximation, the dark electric field can be written as $E \approx \sqrt{\rho_{\rm DM}}\sin(\omega_{\rm s}t - \boldsymbol{k}\cdot\boldsymbol{x})$, where $\rho_{\rm DM} \approx 0.3\,\text{GeV/cm}^3$[21] is the local DM density.

In ground experiments, assume that using a magnet-gravity mechanical oscillator to measure the ultralight DM field along the Earth's axis, we can parameterize the force exerting on the sensor as

$$F_{\rm sig}(t) = \alpha g_{B-L} N_{\rm g} F_0 \sin(\omega_{\rm s}t) \qquad (2)$$

because the de Broglie wavelength of DM is much larger than the size of the sensor so that we drop the x dependence. In this equation, $\alpha = \sin\theta_N$ denotes the component along the direction of gravity and θ_N means the latitude of the location of the ground experiment system. In order to avoid the effects of the Earth's rotation under long time measurements and increase the force, the experiment system is best carried out at high latitudes, e.g., in the Arctic, in which $\alpha = 1$, $F_0 = \sqrt{\rho_{\rm DM}} \approx 10^{-15}\,\text{N}$, and $N_{\rm g}$ is the total number of neutrons in the sensor. We can approximately write it as $N_{\rm g} \approx \frac{1}{2}m/m_{\rm neu}$ in a sensor with mass m and the neutron mass $m_{\rm neu}$. The force $F_{\rm sig}(t)$ is proportional to the mass of the sensor, so the main criterion about the sensor is acceleration sensitivity.

In this Letter, we propose an experiment scheme to detect DM using a frequency-adjustable diamagnetic levitated sensor. The resonance frequency could be changed by adjusting the magnetic field gradient in a paramagnetic

*Corresponding author. Email: hp@nju.edu.cn
© 2023 Chinese Physical Society and IOP Publishing Ltd

part of the oscillator and frequency range from 0.1 Hz to 100 Hz. This means that we have high detection accuracy to detect DM with mass in the range from 10^{-16} eV to 10^{-13} eV. Compared to previously reported experiments, our experiment scheme can achieve improvement in more than one order of magnitude.

Theoretical Calculation. Under the effect of the ultralight DM field, consider thermal noise and measurement noise, the motion equation of a mechanical oscillator at resonant frequency ω_0 could be written as

$$m\ddot{x} + m\gamma\dot{x} + m\omega_0^2 x = F_{\rm sig}(t) + F_{\rm th} + F_{\rm mea}, \tag{3}$$

where γ is damp coefficient; the $F_{\rm sig}(t)$ is the DM field driven by Eq. (2); $F_{\rm th}$ is the environmental thermal noise; and the $F_{\rm mea}$ represents the measurement noise which is mainly composed of the detector imprecision noise and backaction of radiation pressure fluctuations.

The total acceleration noise of the system reads

$$S_{\rm aa}^{\rm tot} = S_{\rm aa}^{\rm th} + \Big(\frac{S_{\rm xx}^{\rm imp}}{|\chi_{\rm m}(\omega,\omega_0)|^2} + \frac{S_{\rm ff}^{\rm ba}}{m^2}\Big), \tag{4}$$

where $\chi_{\rm m}(\omega,\omega_0)$ is the mechanical susceptibility given by $|\chi_{\rm m}(\omega,\omega_0)|^2 = 1/[(\omega^2-\omega_0^2)^2+\gamma^2\omega^2]$, and $S_{\rm aa}^{\rm th} = 4\gamma k_{\rm B}{\rm T}/m$ is the thermal noise where $k_{\rm B}$ is Boltzmann's constant and T indicates environment temperature. The detector imprecision noise $S_{\rm xx}^{\rm imp}$ and the backaction noise $S_{\rm ff}^{\rm ba}$ make up the total measurement noise $S_{\rm aa}^{\rm mea} = S_{\rm xx}^{\rm imp}/|\chi_{\rm m}(\omega,\omega_0)|^2 + S_{\rm ff}^{\rm ba}/m^2$, and $S_{\rm xx}^{\rm imp}\cdot S_{\rm ff}^{\rm ba} = (1/\eta)\hbar^2$ meanwhile. Here $\eta \leqslant 1$ is the measurement efficiency, and $\eta = 1$ corresponds to the standard quantum limit (SQL).

The total measurement noise $S_{\rm aa}^{\rm mea}$ for the sensor operating under the SQL condition at resonance frequency ω_0 could be given by the following simple formula:[22]

$$S_{\rm aa}^{\rm mea,SQL} = \frac{2\sqrt{(\omega_0^2-\omega^2)^2+\gamma^2\omega^2}}{m}. \tag{5}$$

Achieving the SQL in a frequency range needs to optimize the measurement parameters frequency by frequency as the range is scanned.

We use the total acceleration noise $S_{\rm aa}^{\rm tot}$ as the acceleration measurement sensitivity of the system. From Eqs. (2)–(4), considering the optimal case of $\alpha = 1$, we obtain the relationship between coupling strength g_{B-L} and the acceleration measurement sensitivity $S_{\rm aa}^{\rm tot}$ as follows:

$$g_{B-L} = \frac{2m_{\rm neu}}{F_0}\sqrt{\frac{S_{\rm aa}^{\rm tot}}{T_{\rm tot}}}, \tag{6}$$

where $T_{\rm tot}$ denotes the effective total integration time. The DM signal is essentially a coherent force and the timescales $T_{\rm coh} \approx 10^6/\omega_{\rm s}$. When the DM frequency $\omega_{\rm s}$ is lower to satisfy $T_{\rm coh} > T_{\rm mea}$, all the measurement time $T_{\rm mea}$ contributes to the coherent DM signal. As the DM frequency $\omega_{\rm s}$ increases, when $T_{\rm coh} < T_{\rm mea}$, only the proportion of $T_{\rm coh}/T_{\rm mea}$ in the measurement time contributes to the coherent signal. Thus, we define the effective integration time as follows:

$$T_{\rm tot} = \begin{cases} T_{\rm mea}, & \text{if } T_{\rm coh} < T_{\rm mea}, \\ \sqrt{T_{\rm mea}\cdot T_{\rm coh}}, & \text{if } T_{\rm coh} > T_{\rm mea}. \end{cases}$$

Experimental Scheme. The levitated micromechanical and nanomechanical oscillators have been demonstrated to be the ultrasensitive acceleration sensors due to their ultralow dissipation.[23,24] We propose a reasonable scheme by our calculation as shown in Fig. 1(a). A diamagnetic sphere made by PMMA with radius $r_1 = 0.5$ mm (corresponding to volume V_1), density ρ_1 and magnetic susceptibility χ_1 is levitated in the upper magnet (named as magnet A) center region, and the oscillator signal is detected through the fibre on both sides. A paramagnetic microsphere made by Tb_2O_3 with radius $r_2 = 11$ μm (corresponding to volume V_2), density ρ_2 and magnetic susceptibility χ_2 is connected to the upper diamagnetic sphere through a thin glass rod. Another combined magnet (named as magnet B) is placed under the paramagnetic microsphere. The whole magnet assembly is placed in a multi-stage suspension system, and uses active vibration isolation devices to further improve the isolation effect.[25,26]

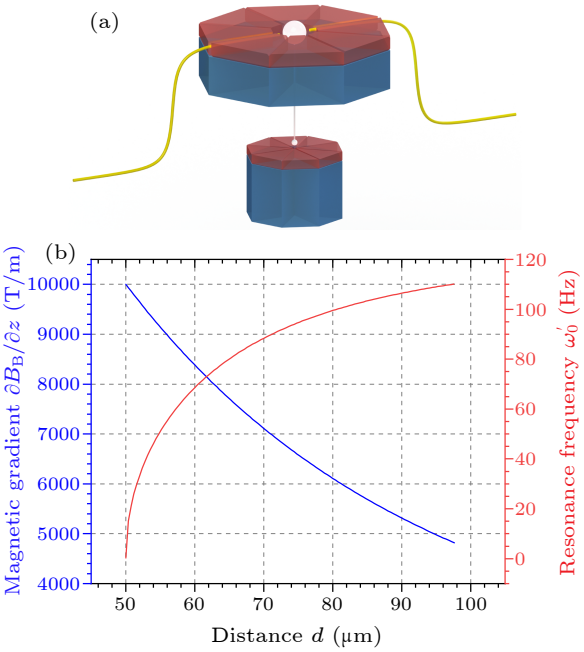

Fig. 1. (a) Schematic diagram of the experimental setup. A diamagnetic sphere of 0.5 mm radius is levitated in the magnetic gravity trap, and a paramagnetic microsphere of 11 μm radius is connected to the upper diamagnetic sphere by a thin glass rod. A 1550 nm laser is transmitted through the left fibre to the right fibre, passing the transparent diamagnetic sphere. (b) The magnetic field gradient $\partial B_{\rm B}/\partial z$ and the resonance frequency ω_0' change by the relative distance d, expressed by the blue and red lines, respectively.

Magnet A is constructed in a way similar to our previous articles.[27] It is necessary to use a high remanence magnetic material with two different magnetization directions to generate enough magnetic force. The red stands for the direction point to the center, and the blue the direction out to the center. In addition, using a less remanence magnetic material to build the upper layer of magnet B and a high magnetic material to build the lower layer. The combination of two different remanence mag-

netic materials allows magnet B to have a higher magnetic field gradient while reducing the magnetic field strength. The direction of magnetization is also indicated by colors of red and blue.

The magnetic field energy of the upper paramagnetic sphere can be written as

$$U_1 = -\int_{V_1} \frac{\chi_1}{2\mu_0} B_{\rm A}^2 \, dV, \tag{7}$$

where $B_{\rm A}$ represents the magnetic field created by magnet A. Assuming that magnet B is far away at beginning, the z direction equilibrium position z_0 of the oscillator in the magnetic-gravity trap satisfies $\partial U_1/\partial z|_{z=z_0} = (\rho_1 V_1 + \rho_2 V_2)g$. The resonance frequency in z direction reads

$$\omega_0 = \sqrt{\frac{1}{\rho_1 V_1 + \rho_2 V_2} \cdot \frac{\partial^2 U_1}{\partial z^2}\bigg|_{z=z_0}}. \tag{8}$$

Then we make magnet B rise, the magnetic field $B_{\rm B}$ from magnet B in the lower paramagnetic microsphere will become larger. Because of $V_2 \ll V_1$, we can simplify the magnetic field energy of the paramagnetic microspheres as $U_2 = -\chi_2 B_{\rm B}^2 V_2/2\mu_0$. Now the resonance frequency along z direction of the oscillator changes to

$$\omega_0' = \sqrt{\omega_0^2 - \frac{\chi_2 V_2}{\mu_0(\rho_1 V_1 + \rho_2 V_2)}\left(\frac{\partial B_{\rm B}}{\partial z}\right)^2\bigg|_{z=z_0}}, \tag{9}$$

where $\chi_2 > 0$ and $\omega_0' < \omega_0$. We ignore the second-order gradient term because of $(\partial B_{\rm B}/\partial z)^2 \gg B_{\rm B}(\partial^2 B_{\rm B}/\partial z^2)$. The magnetic force from magnet B on the paramagnetic microsphere is much lower than the total gravity of oscillator since $B_{\rm B}$ and V_2 are very small. The equilibrium position z_0 will not be changed therefore.

We use the finite element method to simulate the magnetic field gradient $\partial B_{\rm B}/\partial z$ changing with the distance between the paramagnetic microsphere and magnet B expressed by d ranging from 50 μm to 100 μm, then use Eq. (9) to calculate the corresponding resonance frequency ω_0', as shown in Fig. 1(b). It is theoretically possible to bring the resonance frequency ω_0' close to zero by reducing the distance d. However, in order to improve the stability of the oscillator and to reduce the requirement for the isolation system, we select resonance frequency ω_0' variation range from 0.1 Hz to 100 Hz.

Experimental Result Estimation. Now we calculate the acceleration measurement sensitivity of this system. In order to improve the acceleration sensitivity, the whole system was placed in a low temperature environment of $T = 30$ mK, and the damp coefficient is estimated to be $\gamma = 10^{-4}$ Hz.[23,28] In the Supplemental Material, we calculate the dependence of the total measurement noise $S_{\rm aa}^{\rm mea}$ on the laser input power $P_{\rm in}$ and obtain the optimized laser input power $P_{\rm opt}(\omega, \omega_0)$ to minimize the total measurement noise.

In the cases of the oscillator resonance frequency ω_0 equal to 10 Hz and 100 Hz, we calculate the corresponding acceleration noise and present the results in Figs. 2(a) and 2(b). When resonance frequency $\omega_0 = 10$ Hz, we assume measurement efficiency $\eta = 1$ and set the laser input power to optimal laser power for each point as $P_{\rm opt}(\omega, \omega_0)$, as a sequence the measurement noise $S_{\rm aa}^{\rm mea}$ can almost reach the SQL at this time. With the measurement efficiency η reduced to 0.1, the measurement noise is slightly increased. Actually, to simplify the experiment, the laser input power needs to choose near the resonance frequency ω_0 by $P_{\rm opt}(\omega_0, \omega_0)$, it will make the measurement noise $S_{\rm aa}^{\rm mea}$ increase rapidly. In Fig. 2(a), in the frequency range from 9 Hz to 11 Hz, the measurement noise $S_{\rm aa}^{\rm mea}$ is always below the thermal noise $S_{\rm aa}^{\rm th}$ with $\eta = 0.1$. When the resonance frequency ω_0 is adjusted to 100 Hz, the range of measurement noise $S_{\rm aa}^{\rm mea}$ below thermal noise $S_{\rm aa}^{\rm th}$ is reduced to 99.6–100.4 Hz in Fig. 2(b). We can choose an appropriate oscillator resonance frequency scan step $\Delta\omega_0$ from this.

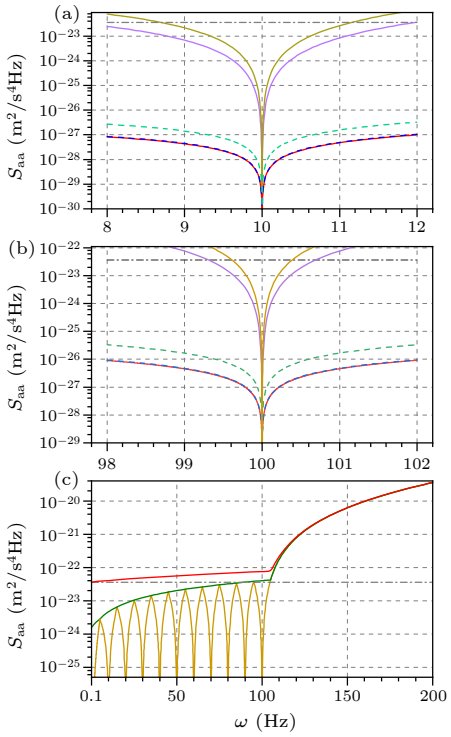

Fig. 2. Acceleration power spectral density $S_{\rm aa}$. (a) Resonance frequency $\omega_0 = 10$ Hz. The grey dashed line indicates the thermal noise $S_{\rm aa}^{\rm th}$; the red line indicates the acceleration detection noise $S_{\rm aa}^{\rm mea,SQL}$; the blue dashed line indicates the $S_{\rm aa}^{\rm mea}$ with the optimal light intensity $P_{\rm opt}(\omega, \omega_0)$ in each frequency between 8 Hz to 12 Hz and the measurement efficiency $\eta = 1$; the green dashed line indicates $P_{\rm opt}(\omega, \omega_0)$ as the same as the blue dashed line but $\eta = 0.1$; the purple line indicates the light intensity $P_{\rm opt}(\omega_0, \omega_0)$ and $\eta = 1$; the yellow line indicates the same $P_{\rm opt}(\omega_0, \omega_0)$ and $\eta = 0.1$. (b) The same as (a) but $\omega_0 = 100$ Hz. (c) Resonance frequency ω_0 adjusted from 0.1 Hz to 100 Hz. The grey dashed line indicates the thermal noise $S_{\rm aa}^{\rm th}$; the yellow line indicates the acceleration measurement noise $S_{\rm aa}^{\rm mea}$ with $\eta = 0.1$, and here the scan step $\Delta\omega_{\rm s} = 10$ Hz is only used to show the measurement scheme; the green line indicates the envelope of the yellow line in the diagram and it is written as $S_{\rm aa}^{\rm mea'}$; the red line is the acceleration measurement sensitivity $S_{\rm aa}^{\rm tot} = S_{\rm aa}^{\rm th} + S_{\rm aa}^{\rm mea'}$.

According to the calculation results from Figs. 2(a) and 2(b), we choose the scan step $\Delta\omega_0 = 1$ Hz in the region

resonance frequency ω_0 range from 0.1 Hz to 100 Hz, and each scan covers the frequency range from $\omega_0 - \Delta\omega_0/2$ to $\omega_0+\Delta\omega_0/2$, fixing the laser input power $P_{\rm in} = P_{\rm opt}(\omega_0, \omega_0)$ in each scan meanwhile. We calculate the acceleration measurement noise $S_{\rm aa}^{\rm mea}$ with $\eta = 0.1$ in each scan, and calculate the envelope of these series $S_{\rm aa}^{\rm mea}$ written as $S_{\rm aa}^{\rm mea'}$. The acceleration measurement sensitivity $S_{\rm aa}^{\rm tot} = S_{\rm aa}^{\rm th} + S_{\rm aa}^{\rm mea'}$, and these results are presented in Fig. 2(c).

According to the above discussion on the effective integration time $T_{\rm tot}$, we fix the measurement time of each scan as $T_{\rm mea} = 10^5$ s. When DM frequency $\omega_{\rm s} < 10$ Hz, $T_{\rm tot} = T_{\rm mea}$; and when $\omega_{\rm s} > 10$ Hz, $T_{\rm tot} = \sqrt{T_{\rm mea} \cdot 10^6/\omega_{\rm s}}$. Combining the above discussion of the scan step, we estimate that about one hundred times of adjustments and measurements will be required in total, corresponding to a total time of 1×10^7 s. The final result of coupling strength g_{B-L} from Eq. (6) is shown in Fig. 3. In the region of $\omega_{\rm s} < 100$ Hz, this system always has high acceleration sensitivity by adjusting the resonance frequency of the mechanical oscillator. We achieve more than one order of magnitude improvement in the measurement of g_{B-L} compared to the MICROSCOPE and the Eöt–Wash torsion experiment. In the region of $\omega_{\rm s} > 100$ Hz, the measurement accuracy of g_{B-L} decreases rapidly, due to the increase in measurement noise $S_{\rm aa}^{\rm mea}$.

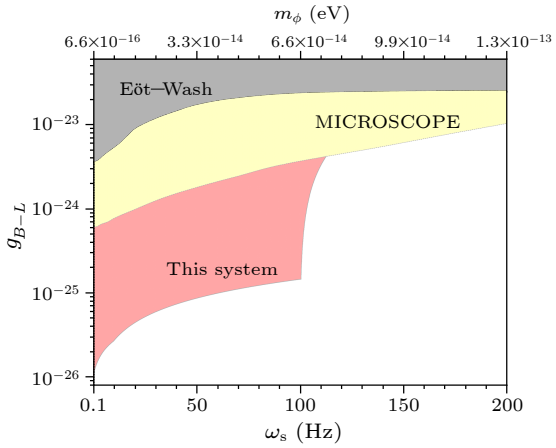

Fig. 3. Ultra-light dark matter search range. The top axis represents the DM mass m_ϕ corresponding to the frequency $\omega_{\rm s}$. The upper grey and yellow regions are excluded by Eöt–Wash torsion balance [29–31] and MICROSCOPE experiments, [32,33] and the red region is the range this system can cover. In the torsion balance system, they use a pair of accelerometers (beryllium and titanium, i.e., Be and Ti) with a differential neutron/nucleon ratio $\Delta = N_1/A_1 - N_2/A_2 = 0.037$, where N and A are the neutron and nucleon numbers of Be and Ti, respectively. From Eq. (2), $N_{\rm g}$ can be approximated as $N_{\rm g} = \Delta \cdot m/m_{\rm neu}$ at this time.

Finally, we estimate the minimal g_{B-L} this system can detect. Assume that the DM frequency $\omega_{\rm s}$ is 1 Hz, 10 Hz, and 100 Hz respectively. From Eq. (6) and the measurement time $T_{\rm mea}$ ranging from 10^3 s to 10^7 s, the results are shown in Fig. 4. When $T_{\rm mea}$ is less than the coherent time $T_{\rm coh}$, g_{B-L} decreases rapidly as $T_{\rm mea}$ increases; and when $T_{\rm mea}$ is greater than $T_{\rm coh}$, g_{B-L} decreases more slowly. If the final measurement time is about 10^7 s, the minimal g_{B-L} that can be taken as the measurement scale is about 10^{-26}.

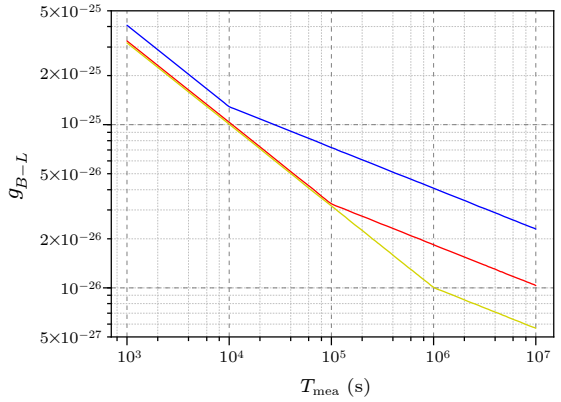

Fig. 4. The minimal g_{B-L} can be reached in different DM frequencies $\omega_{\rm s}$. The yellow, red, and blue lines indicate $\omega_{\rm s}$ of 1 Hz, 10 Hz, and 100 Hz, respectively. The maximum measurement time is 10^7 s (about 115.7 days).

In summary, we have proposed an experimental scheme to detect ultra-light dark matter using a frequency-adjustable diamagnetic levitated microsphere sensor which can theoretically approach the standard quantum limit. We change the resonance frequency by adjusting the distance between the paramagnetic microsphere and the lower combined magnets, and to obtain a lager range that maintains high acceleration measurement sensitivity. Compared to the existing system, our method can achieve at least one order of magnitude improvement in the coupling constant g_{B-L}, especially in the frequencies from 0.1 Hz to 100 Hz. It may be possible to achieve higher accuracy by using the array of sensors in the future.

In this work, we consider only the effects of thermal noise and quantum measurement noise on the acceleration measurement sensitivity of the system. In fact, there are many low-frequency noises such as seismic waves and Earth tidal forces which also have a great impact on the accuracy of the experiment, which cannot be shielded by the suspension system. This poses a great challenge to the actual measurement. Reducing the frequency scan step according to the accuracy of the active vibration isolation device may make the effect of other noise lower than thermal noise, and this needs to be verified by further experiments.

In general, the current ground-based precision measurement system may have a broader prospect in terms of dark matter measurement compared to the previous astronomical observation methods. In the future, with the development of measurement sensitivity and measurement range of mechanical sensors, especially with the improvement quantum sensing technology, the measurement sensitivity may break through the standard quantum limit. It will open up more possibilities in terms of dark matter measurement.

Acknowledgments. This work was supported by the National Natural Science Foundation of China (Grant Nos. 12205291, 12075115, 12075116, 11890702, and 12150011), the Fundamental Research Funds for the Cen-

tral Universities, and Anhui Provincial Natural Science Foundation (Grant No. 2208085QA16).

References

[1] Sofue Y and Rubin V 2001 *Annu. Rev. Astron. Astrophys.* **39** 137
[2] Massey R, Kitching T, and Richard J 2010 *Rep. Prog. Phys.* **73** 086901
[3] Markevitch M, Gonzalez A H, Clowe D, Vikhlinin A, Forman W, Jones C, Murray S, and Tucker W 2004 *Astrophys. J.* **606** 819
[4] Gianfranco B 2010 *Particle Dark Matter: Observations, Models and Searches* (Cambridge: Cambridge University Press)
[5] Tanabashi M, Hagiwara K, Hikasa K *et al.* (Particle Data Group Collaboration) 2018 *Phys. Rev. D* **98** 030001
[6] Irastorza I G and Redondo J 2018 *Prog. Part. Nucl. Phys.* **102** 89
[7] Hui L, Ostriker J P, Tremaine S, and Witten E 2017 *Phys. Rev. D* **95** 043541
[8] Bovy J, Prieto C A, Beers T C *et al.* 2012 *Astrophys. J.* **759** 131
[9] O'Hare C A J, McCabe C, Evans N W, Myeong G, and Belokurov V 2018 *Phys. Rev. D* **98** 103006
[10] Myeong G C, Evans N W, Belokurov V, Amorisco N C, and Koposov S E 2018 *Mon. Not. R. Astron. Soc.* **475** 1537
[11] Du N, Force N, Khatiwada R *et al.* (ADMX Collaboration) 2018 *Phys. Rev. Lett.* **120** 151301
[12] Backes K M, Palken D A, Kenany S A *et al.* 2021 *Nature* **590** 238
[13] Kwon O, Lee D, Chung W *et al.* 2021 *Phys. Rev. Lett.* **126** 191802
[14] Abel C, Ayres N J, Ban G *et al.* 2017 *Phys. Rev. X* **7** 041034
[15] Terrano W A, Adelberger E G, Hagedorn C A, and Heckel B R 2019 *Phys. Rev. Lett.* **122** 231301
[16] Smorra C, Stadnik Y, Blessing P *et al.* 2019 *Nature* **575** 310
[17] Kennedy C J, Oelker E, Robinson J M, Bothwell T, Kedar D, Milner W R, Marti G E, Derevianko A, and Ye J 2020 *Phys. Rev. Lett.* **125** 201302
[18] Arvanitaki A, Huang J, and Van Tilburg K 2015 *Phys. Rev. D* **91** 015015
[19] Vermeulen S M, Relton P, Grote H *et al.* 2021 *Nature* **600** 424
[20] Carney D, Hook A, Liu Z, Taylor J M, and Zhao Y 2021 *New J. Phys.* **23** 023041
[21] Read J I 2014 *J. Phys. G: Nucl. Part. Phys.* **41** 063101
[22] Clark J B, Lecocq F, Simmonds R W, Aumentado J, and Teufel J D 2017 *Nature* **541** 191
[23] Leng Y, Li R, Kong X, Xie H, Zheng D, Yin P, Xiong F, Wu T, Duan C K, Du Y, Yin Z Q, Huang P, and Du J 2021 *Phys. Rev. Appl.* **15** 024061
[24] Monteiro F, Li W, Afek G, Li C L, Mossman M, and Moore D C 2020 *Phys. Rev. A* **101** 053835
[25] Acernese F, Antonucci F, Aoudia S *et al.* 2010 *Astropart. Phys.* **33** 182
[26] Acernese F, Agathos M, Agatsuma K *et al.* 2015 *Class. Quantum Grav.* **32** 024001
[27] Zheng D, Leng Y, Kong X, Li R, Wang Z, Luo X, Zhao J, Duan C K, Huang P, Du J, Carlesso M, and Bassi A 2020 *Phys. Rev. Res.* **2** 013057
[28] Xiong F, Yin P, Wu T, Xie H, Li R, Leng Y, Li Y, Duan C, Kong X, Huang P, and Du J 2021 *Phys. Rev. Appl.* **16** L011003
[29] Wagner T A, Schlamminger S, Gundlach J H, and Adelberger E G 2012 *Class. Quantum Grav.* **29** 184002
[30] Schlamminger S, Choi K Y, Wagner T A, Gundlach J H, and Adelberger E G 2008 *Phys. Rev. Lett.* **100** 041101
[31] Arvanitaki A, Dimopoulos S, and Van Tilburg K 2016 *Phys. Rev. Lett.* **116** 031102
[32] Hees A, Minazzoli O, Savalle E, Stadnik Y V, and Wolf P 2018 *Phys. Rev. D* **98** 064051
[33] Bergé J, Brax P, Métris G, Pernot-Borràs M, Touboul P, and Uzan J P 2018 *Phys. Rev. Lett.* **120** 141101